Influence of Al concentration on the optoelectronic properties of Al-doped MgO

N. Sarmadian, R. Saniz, D. Lamoen, and B. Partoens

CMT & EMAT, Departement Fysica, Universiteit Antwerpen, Groenenborgerlaan 171, B-2020 Antwerpen, Belgium

We use density functional theory within the local density approximation to investigate the structural, electronic, and optical properties of Al-doped MgO. The concentrations considered range from 6% to 56%. In the latter case, we also compare the optical properties of the amorphous and crystalline phases. We find that, overall, the electronic properties of the crystalline phases change qualitatively little with Al concentration. On the other hand, the changes in the electronic structure in the amorphous phase are more important, most notably because of deep impurity levels in the band gap that are absent in the crystalline phase. This leads to observable effects in, e.g., the optical absorption edge and in the refractive index. Thus, the latter can be used to characterize the crystalline to amorphous transition with Al doping level.

PACS number(s): 71.15.Mb, 78.20.Ci, 71.20.Nr

I. INTRODUCTION

Because of their very rich phenomenology,[1] transition-metal oxides, either stoichiometric or doped, are the subject of extensive research efforts worldwide and play a central role in present-day technology. A simple compound such as MgO (magnesia), for example, was long used for its optical properties (being famously commercialized by Eastman-Kodak under the name Itran-5),[2] and is currently a key element of plasma display devices because of its large secondary electron emission coefficient and its simultaneous role as an insulating layer.[3] Doped MgO has also attracted interest in different respects. Indeed, *p*-type doping has been investigated in Li-doped MgO,[4] as well as magnetism in N-doped MgO,[5] and cathodoluminescence in Cr-doped MgO,[6] to name a few examples. Very recently, there has been theoretical and experimental interest in Al-doped MgO.[7–10] In these works, a magnetron sputtering technique was used to grow Al-doped MgO thin films, with Al substituting Mg, for a wide range of Al concentrations. An interesting finding is that both molecular dynamics simulations and experiment indicate that crystallinity is retained up to around 40% to 50% Al doping (depending on the substrate), beyond which level the system becomes amorphous.[7,9] Measured properties such as hardness, refractive index, and others were observed to vary correspondingly.[8]

For a more complete characterization of experimentally grown films and for a better understanding of their properties, theoretical studies are of great assistance. In this work, we perform a first-principles study of these systems to try to shed light on how their properties change with varying Al content. We consider crystalline phases with Al doping concentrations ranging from 6% to 56%. In the latter case, we also model an amorphous structure. In the crystalline phases we find that, remarkably, the film electronic properties are overall qualitatively robust with respect to Al concentration. Indeed, although the quantitative changes with Al concentration can be important, the properties considered remain qualitatively similar. This is in stark contrast with what we find in the amorphous case. In the 56% doped amorphous structure there are impurity levels deep in the band gap, which are not present in the crystalline phases at any of the doping levels we studied. A clear consequence of this is a series of sharp peaks in the

optical absorption edge in the amorphous case, completely absent in the crystalline phases. Thus, there is a significant redshift of the absorption edge with Al concentration. As a further observable consequence, the optical dielectric constant and the refractive index change in a significant way. These effects can be considered additional signatures of the transition from the crystalline to the amorphous phase in these systems.

This report is organized as follows. In Sec. II we present the methodology used, and in Sec. III we present our results together with a discussion. In Sec. IV we summarize our main findings.

II. COMPUTATIONAL METHOD

Our simulations are performed using density functional theory (DFT)[11,12] as implemented in the plane-wave Vienna *Ab initio* Simulation Package (VASP).[13,14] We used the local density approximation (LDA) with the Ceperley-Alder parametrization[15] and projector augmented wave (PAW) potentials.[16,17] The Mg $2p$ $3s$, O $2s$ $2p$, and Al $3s$ $2p$ orbitals were treated as valence. An energy cutoff of 450 eV was used for the plane-wave basis set. For structure relaxation and total energy calculations the Brillouin zone was sampled using a $3 \times 3 \times 3$ Monkhorst-Pack (MP) grid.[18] Doping is studied by using a 64-atom supercell, consisting of $2 \times 2 \times 2$ conventional cubic cells. To keep the cation-anion charge balance, doping obeys to $Mg_{1-3x/2}Al_xO$. Thus, for every two Al atoms introduced, there is one Mg vacancy with respect to the original rocksalt structure. For each Al concentration, x, we considered three different possible (not exhaustive) configurations. The Al atom distribution was uniform, but random.[19] In all cases, the calculations were made at the equilibrium lattice constants. Atomic relaxations were made until residual forces on the atoms were less than 0.01 eV/Å and total energies were converged within 1 meV.

The imaginary part of the dielectric function (tensor) is obtained using the random phase approximation, as implemented in the VASP code.[20,21] The real part of the dielectric function is obtained from the imaginary part through the Kramers-Kronig relation. For each doping concentration, we averaged the dielectric function over all considered configurations. The results were also averaged with respect to the direction of

polarization. We found that it is enough to sample the Brillouin zone using a $6 \times 6 \times 6$ MP grid for our supercell to obtain a converged $\varepsilon(\omega)$ tensor. We increased the number of bands up to 320 in order to guarantee a converged dielectric function in the 0–45 eV energy range.

III. RESULTS AND DISCUSSION

A. Crystalline structures

We model first crystalline structures, and study the lattice parameters' dependence on Al concentration. Here the concentration is given by ratio of the number of Al atoms over the number of Al plus Mg atoms in the supercell. The Al concentrations considered are 6%, 13%, 21%, 29%, 37%, and 56%. Figure 1(a) shows the dependence of the supercell lattice vector lengths (a, b, and c) on Al concentration. The vector lengths are divided by 2 to compare to the result of pure MgO. The dependence is shown for three different possible configurations considered, for each Al content level. The solid lines indicate the averages over the three configurations. These can be expected to be closer to what is found in experiment. Figure 1(b) shows a similar plot for the angles (α, β, and γ) between the supercell primitive vectors. As one can see in the figures, the averages indicate that the crystal structure remains approximately cubic up to an Al content of 30% to 37%. Above that value, there is a very clear departure from a cubic structure. This is interesting, because in experiment there is a transition from the crystalline to an amorphous phase for an Al concentration between 40% and 50% (depending on whether the films are deposited on an amorphous or crystalline substrate).[7,9] We think that both of the above observations are related to an increasing instability of the rocksalt structure with increasing Al concentration. In this respect, we note the following. First, the x-ray diffraction measurements in Ref. 9 indicate a crystallinity fraction with respect to the rocksalt structure (space group $Fm\bar{3}m$) that decreases with Al concentration. Second, the molecular dynamics calculated radial distribution functions for the different bonds are not completely consistent with the MgO crystal structure, with the Al-O radial distribution function deviating from it.[7] The thermodynamic ground state of the doped system is expected to present phase segregation into MgO and $MgAl_2O_4$. However, according to Saraiva and co-workers the experimental structures are kinetically

determined, and not thermodynamically, because of a too low adatom mobility during deposition.[9] Kinetic barriers also trap our *ab initio* structures in local energy minima, away from the thermodynamic ground state. Hence, we can expect the theoretical structures to be reasonably close to the experimental ones. Thus, in Fig. 1 one can see that the average lattice constant (average of the three primitive vector lengths) decreases approximately linearly with increasing Al content. This is in agreement with experiment, where it is concluded that the lattice parameter dependence on Al concentration follows Vegard's law.[9] This can be understood as due to the smaller Al radius compared to Mg and to the increasing number of vacancies in the supercells with increasing Al content.

We turn now to the dependence of the electronic properties on the Al doping level. We found that the system is insulating for all the doping concentrations considered. In Fig. 2(a) we show the band gap as a function of Al concentration. The different configurations can show very different gaps, but in films that are several hundred nm to 1 μm thick, only an average can be observed experimentally. The average over the different configurations considered here is given by the solid line. The band gaps show a clear tendency to decrease with increasing Al concentration, and this leads to an almost monotonic decrease of the average band gap. The average band gap falls by near 25% from the calculated MgO value, roughly 5 eV, to the ~3.8 eV value at 56% doping. At this point we recall that the LDA can severely underestimate band gaps. In the case of MgO, the calculated band gap is to be compared with the experimental value of 7.8 eV.[22] However, the trends in the dependence of the band gap on lattice parameters are considered to be described quite reliably by the DFT-LDA scheme used here.[23,24]

The fact that the band gap has a tendency to decrease with Al concentration obeys two facts. First, both valence and conduction band widths increase with Al content. To show this,
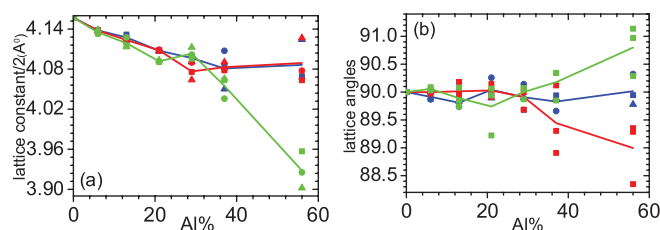

FIG. 1. (Color online) Lattice constants (a) and angles between the lattice vectors (b) as a function of Al concentration. The blue, red, and green colors correspond to the lattice constants a, b, and c in (a) and the angles α, β, and γ in (b). For every concentration, three configurations are considered. The lines correspond to the average value.
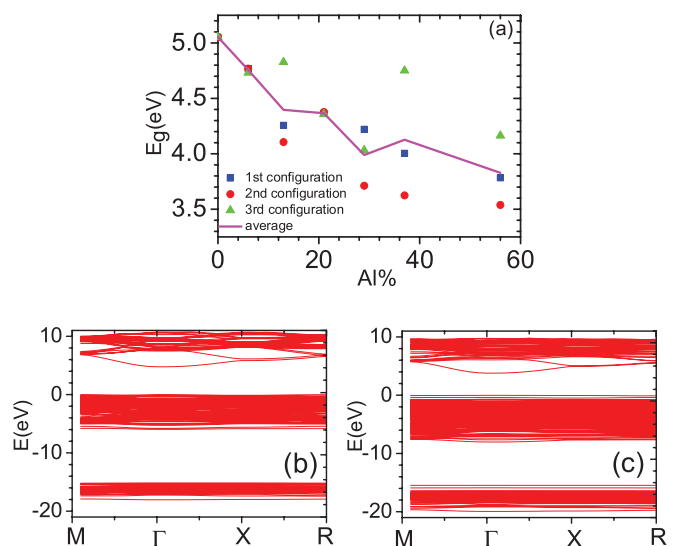

FIG. 2. (Color online) (a) Band gap dependence on the Al concentration. (b) Band structure for 6% Al-doped MgO, and similar in (c) for 56% Al-doped MgO. There is a notable increase in band widths at higher doping level.
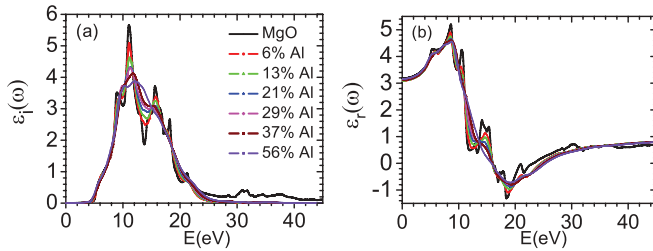
FIG. 3. (Color online) Influence of Al concentration on (a) imaginary part and (b) real part of the dielectric function of Al-doped MgO.

we plot the band structure for Al concentrations of 6% and 56% (for one of the possible configurations) in Figs. 2(b) and 2(c), respectively. Second, doping with Al creates O-like acceptor states, just above the valence band maximum. They are created by the Mg vacancies and passivated by the Al electrons. These states tend to detach more from the valence band continuum with increasing doping concentration, thus contributing further to the band gap narrowing. This is also illustrated in Figs. 2(b) and 2(c). Furthermore, as can be seen in these figures, for higher Al content, the eigenvalue distribution as a function of **k** point and band tends to be more homogeneous than for lower Al content, reflecting the lower symmetry of the former case. This has an influence on the optical spectra peak structure, as discussed below.

Of interest in experiment has been the refractive index.[8] Therefore, we consider dependence on Al concentration of the average dielectric function. Figures 3(a) and 3(b) show the imaginary (ε_i) and real (ε_r) parts, respectively, for the different Al concentrations we are studying here. For reference, the dielectric function for MgO is also plotted. In both figures one can clearly see that the rather sharp structure in the spectrum for low Al content gradually disappears as Al concentration increases. This can be understood by considering the evolution of the density of states (DOS) with Al concentration. Indeed, due to a more homogeneous eigenvalue distribution (within each band manifold) among **k** points in the Brillouin zone [cf. Figs. 2(b) and 2(c)], the structure in the DOS itself tends to disappear as the Al content increases. This is shown in Figs. 4(a) and 4(b), where we plot the total DOS corresponding to Figs. 2(b) and 2(c). The joint density of states will show a similar behavior and will result in the trends seen in Fig. 3. The broader band widths for higher Al content, also reflected in the DOS, will contribute further to a smoother dielectric function as a function of energy.
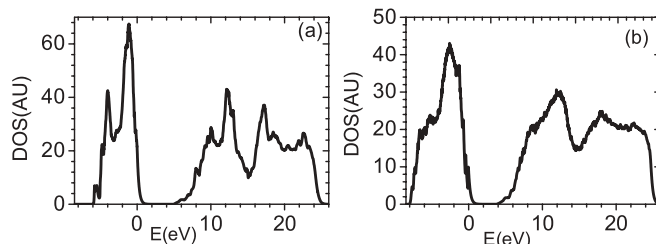

FIG. 4. DOS plots for (a) 6% and (b) 56% Al-doped MgO. At higher doping level, the fine structure in the density of states tends to disappear.
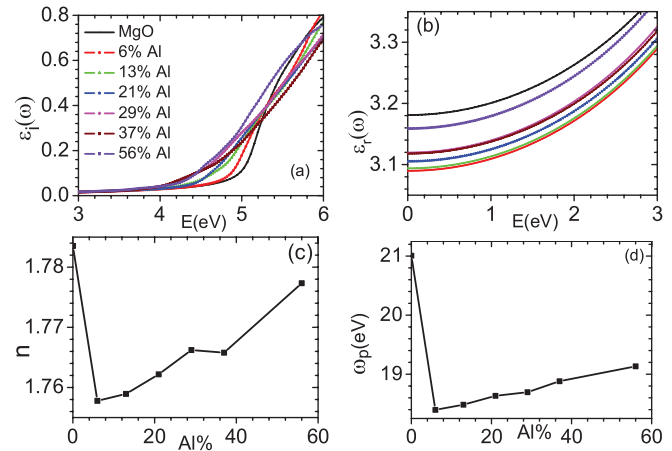

FIG. 5. (Color online) (a) Change in the imaginary part of the dielectric function of Al-doped MgO around the absorption edge varying Al concentration. (b) Low-frequency dependence of the real part of the dielectric function for the different Al concentrations considered in this work. (c) and (d) Dependence of the refractive index and plasma frequency, respectively, on Al concentration.

Consider now the low-frequency behavior of the dielectric function. There are two aspects that are relevant to experiment. One is the absorption edge, essentially determined by onset of the imaginary part of the dielectric function. The other is the zero-frequency limit of the real part of the dielectric function, i.e., the optical dielectric constant. In Fig. 5(a), we consider the evolution of the absorption edge with Al concentration. Comparing with Fig. 2(a), one can see that the absorption edge is correlated directly with the band gap, as can be expected. The absorption edge width gradually increasing with Al concentration can be attributed to the corresponding decrease of crystalline order. Figure 5(b) shows the low-frequency behavior of the real part of the dielectric function as a function of Al doping level. One can see that ε_∞ drops as soon as Al replaces some of the Mg atoms. This indicates that the polarizability of the system tends to be reduced with respect to MgO. However, the drop is rather small compared to the absolute value of the dielectric constants. Note that our result $\varepsilon_\infty \simeq 3.18$ is reasonably close to the experimental value of 3.[25] The slight overestimation can be mainly attributed to the underestimation of the band gap.

The low-frequency limit of the refractive index is given by $n = \sqrt{\varepsilon_r(0)}$. This is plotted in Fig. 5(c), where one can see a tendency to increase with Al concentration. The same tendency is observed in experiment up to 40% Al doping, although our values are between 7% and 11% higher than the measured values.[8] For an Al concentration higher than 40%, our results cannot be directly compared with experiment. In the latter, the phase is amorphous, while in our calculations it is not. On the other hand, it should be noted that the accuracy of the experimental values is not completely clear. For instance, for a pure MgO crystal, the optical dielectric constant value is 3.[25] We find a value of 3.18, as mentioned above, against a value of around 3.5 in experiment.[8]

To conclude this subsection, we consider another quantity that can be used to characterize a system, namely, the plasma frequency, ω_p. It can be readily calculated from the dielectric
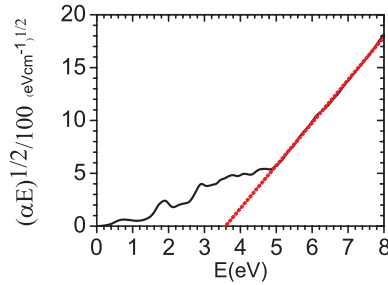
FIG. 6. (Color online) Tauc plot for pseudoamorphous 56% Al-doped MgO.

function using the well-known sum rule

$$\frac{\pi}{2}\omega_p^2 = \int_0^\infty d\omega\, \omega\varepsilon_i(\omega). \tag{1}$$

Here we study the dependence on Al concentration of the plasma frequency averaged also over the three spatial directions. The results are plotted in Fig. 5(d). One can clearly see that ω_p increases with Al content. Given that the number of valence electrons is independent of Al content, the increase of ω_p can be understood as a consequence of the reduction of the lattice constant with increasing Al concentration. We verified that the valence electron density gives plasma frequencies very close to those determined with the sum rule above.

B. Amorphous versus crystalline structure

As indicated above, experiment and molecular dynamics simulations show that an Al doping concentration larger than 40% to 50% leads to an amorphous system.[7,9] Snapshots of the molecular dynamics simulations are found in Ref. 7. We note that these show no indication of phase segregation as the Al content increases. In this last subsection, we consider 56% Al-doped MgO in the amorphous and crystalline structures, and compare their structural and optical properties. To model the amorphous structure we proceed as follows. Data from molecular dynamics simulations for a supercell containing 11 Mg, 13 Al, and 32 O atoms were obtained.[10] In our calculations, one Al atom was added to that structure in order to obtain a charge-balanced system. We then constructed two additional configurations by completely randomly changing the positions of Al and Mg atoms in the charge-balanced system. The supercell size and atomic positions of the pseudoamorphous structures corresponding to these three configurations were were fully optimized. In the following, we consider the averaged properties of these three structures as representative of an amorphous structure. The amorphous supercell size thus obtained is 8.279 Å, compared to 8.066 Å for the crystalline structure. The larger supercell size in the former case (larger by 2.6%) is due to the increased disorder in this structure.

The optical gap of the amorphous structure can be determined by means of a Tauc plot, which is commonly used to determine the optical gap of amorphous materials.[26] One plots $(E\alpha)^{1/2}$ versus E (cf. Fig. 6), with E the photon energy and α the optical absorption coefficient given by

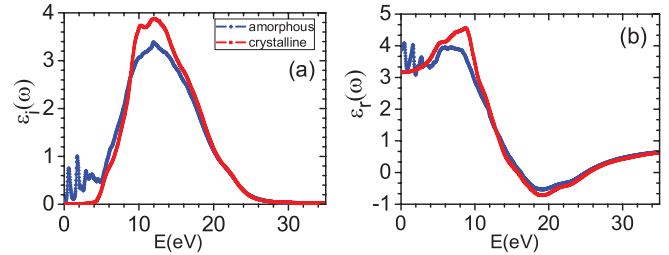$$\alpha = \frac{4k\pi}{\lambda}, \tag{2}$$

FIG. 7. (Color online) Frequency dependence of the calculated dielectric function (a) $\varepsilon_i(\omega)$ and (b) $\varepsilon_r(\omega)$, comparing the crystalline and amorphous cases in 56% Al-doped MgO.

where λ is the photon wavelength and k is the extinction coefficient

$$k = \sqrt{\frac{-\epsilon_r + \sqrt{\epsilon_r^2 + \epsilon_i^2}}{2}}. \tag{3}$$

Extrapolating the linear regime in the plot to the abcissa yields the optical gap, as shown in Fig. 6. We thus obtain an optical gap of 3.56 eV. For reference, we note that the band gap of the crystalline structure is 3.85 eV. For further comparison, in Figs. 7(a) and 7(b), we plot the imaginary and real parts of the dielectric function, respectively, for both structures. The plots reflect immediately a fundamental difference in the electronic structure of two systems, namely, the disorder-induced states in the band gap in the amorphous case. The latter produce the absorption peaks below 5 eV in ε_i in Fig. 7(a). To discuss this further, we plot the corresponding density of states in Figs. 8(a) and 8(b). We note that the states in the gap are robust; i.e., averaging over different disordered configurations tends to broaden their overall energy spread, but does not really weaken their effect.

Figure 8(a) clearly shows two localized states in the gap in the amorphous phase just above the Fermi level (0 eV). Finally, we comment that we find the optical dielectric constant for the amorphous system is 3.87, to compare with 3.16 for the crystalline system. Using the Clausius-Mossotti relation,[25] one can readily deduce that the polarizability of the amorphous phase is 26% higher than in the crystalline phase. The higher polarizability in the amorphous phase may be due to the weakening of the bond strength in the amorphous phase. This is in line with our finding above, that the band gap in the amorphous phase is smaller than in the crystalline phase.[27] We also calculated the plasma frequency in the amorphous phase. We find it is 18.10 eV, which is smaller than the 19.13 eV value for the crystalline system (cf. Fig. 7). Given that the valence
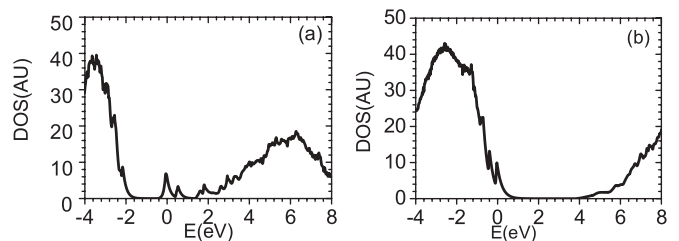

FIG. 8. density of states (DOS) for (a) amorphous and (b) crystalline 56% Al-doped MgO.

charge in both systems is the same, this can be understood as due to the larger supercell size in the amorphous case (i.e., lower electron density). This is similar to what is observed in other amorphous systems, such as amorphous carbon.[28]

IV. DISCUSSION AND SUMMARY

It is interesting that the results in the previous section show that the electronic properties of crystalline Al-doped MgO are rather robust against doping level. Indeed, although the band gap, dielectric function, and related properties show quantitative changes upon changing the Al concentration, the changes are nearly monotonic. This implies that the electronic properties do not change qualitatively in a really significant way. It is only when one considers the amorphous phase that one finds a more significant change in the electronic properties. The most important effect is the appearance of impurity levels deep in the band gap. There are several observable consequences of this. We mention, in particular, the

important redshift of the optical absorption edge, due to these levels, and the related sudden drop of the band gap. A further consequence is an equally sudden jump upward of ε_∞ and of the refractive index. Thus, these effects can be considered as a further signature of the transition from the crystalline to the amorphous phase in these systems. As such, they provide additional criteria for the experimental characterization of the crystalline/amorphous transition.

[1] S. Maekawa, T. Tohyama, S. E. Barnes, S. Ishihara, W. Koshibae, and G. Khaliullin, *Physics of Transition Metal Oxides* (Springer-Verlag, Berlin, 2004).

[2] D. C. Harris, Infr. Phys. Technol. **39**, 185 (1998).

[3] J. P. Beouf, J. Phys. D: Appl. Phys. **36**, R53 (2003).

[4] M. M. Tardío, R. Ramírez, R. González, and Y. Chen, Phys. Rev. B **66**, 134202 (2002).

[5] M. Pesci, F. Gallino, C. Di Valentin, and G. Pacchioni, J. Phys. Chem. C **114**, 1350 (2010).

[6] F. Stavale, N. Nilius, and H.-J. Freund, New J. Phys. **14**, 033006 (2012).

[7] V. Georgieva, M. Saraiva, N. Jehanathan, O. I. Lebedev, D. Depla, and A. Bogaerts, J. Phys. D: Appl. Phys. **42**, 065107 (2009).

[8] M. Saraiva, H. Chen, W. P. Leroy, S. Mahieu, N. Jehanathan, O. Lebedev, V. Georgieva, R. Persoons, and D. Depla, Plasma Process. Polym. **6**, 5751 (2009).

[9] M. Saraiva, V. Georgieva, S. Mahieu, K. Van Aeken, A. Bogaerts, and D. Depla, J. Appl. Phys. **107**, 034902 (2010).

[10] V. Georgieva, I. T. Todorov, and A. Bogaerts, Chem. Phys. Lett. **485**, 315 (2010).

[11] P. Hohenberg and W. Kohn, Phys. Rev. **136**, B864 (1964).

[12] W. Kohn and L. J. Sham, Phys. Rev. **140**, A1133 (1965).

[13] G. Kresse and J. Hafner, Phys. Rev. B **47**, R558 (1993); J. Phys.: Condens. Matter **6**, 8245 (1994).

[14] G. Kresse and J. Furthmüller, Comput. Mater. Sci. **6**, 15 (1996); Phys. Rev. B **54**, 11169 (1996).

[15] D. M. Ceperley and B. J. Alder, Phys. Rev. Lett. **45**, 566 (1980).

[16] G. Kresse and D. Joubert, Phys. Rev. B **59**, 1758 (1999).

[17] P. E. Blöchl, Phys. Rev. B **50**, 17953 (1994).

[18] H. J. Monkhorst and J. D. Pack, Phys. Rev. B **13**, 5188 (1976).

[19] In Ref. 7, one can see that the Al atoms show no signs of clustering, independently of the substrate used.

[20] B. Adolph, J. Furthmüller, and F. Bechstedt, Phys. Rev. B **63**, 125108 (2001).

[21] M. Gajdos, K. Hummer, G. Kresse, J. Furthmüller, and F. Bechstedt, Phys. Rev. B **73**, 045112 (2006).

[22] U. Schönberger and F. Aryasetiawan, Phys. Rev. B **52**, 8788 (1995).

[23] S. K. Yadav, T. Sadowski, and R. Ramprasad, Phys. Rev. B **81**, 144120 (2010).

[24] L. Dong, S. K. Yadav, R. Ramprasad, and S. P. Alpay, Appl. Phys. Lett. **96**, 202106 (2010).

[25] N. W. Ashcroft and N. D. Mermin, *Solid State Physics* (Saunders College, Forth Worth, 1976).

[26] K. Morigaki, *Physics of Amorphous Semiconductors* (Imperial Collage Press, 1999).

[27] G. A. N. Connell, in *Amorphous Semiconductors*, edited by M. H. Brodsky (Springer, Berlin, 1979), p. 73.

[28] J. T. Titantah and D. Lamoen, Phys. Rev. B **70**, 033101 (2004).